DOI: 10.1021/ma100669g

Macromolecules
ARTICLE

Role of Surface Interactions in the Synergizing Polymer/Clay Flame Retardant Properties

Seongchan Pack,*,† Takashi Kashiwagi,‖ Changhong Cao,§ Chad S. Korach,§ Menachem Lewin,⊥ and Miriam H. Rafailovich*,†,‡

†*Department of Materials Science and Engineering,* ‡*Chemical and Molecular Engineering Program, and* §*Department of Mechanical Engineering, State University of New York at Stony Brook, Stony Brook, New York 11794,* ‖*Fire Research Division, National Institute of Standards and Technology, Gaithersburg, Maryland 20899-8665, and* ⊥*Polytechnic University, Polymer Research Institute, Department of Chemical and Biological Sciences, 6 Metrotech Center, Brooklyn, New York 11201*

Received March 28, 2010; Revised Manuscript Received May 8, 2010

ABSTRACT: The absorption of resorcinol di(phenyl phosphate) (RDP) oligomers on clay surfaces has been studied in detail and is being proposed as an alternative method for producing functionalized clays for nanocomposite polymers. The ability of these clays to be exfoliated or intercalated in different homopolymers was investigated using both transmission electron microscopy and small-angle X-ray scattering results, compared with contact angle measurements on Langmuir−Blodgett clay monolayers, where the interfacial energies were used as predictors of the polymer/clay interactions. We found that the contact angle between PS/RDP clay monolayer substrates was ∼2.5°, whereas the angle for polystyrene (PS)/Cloisite 20A clays substrates was ∼32°, consistent with the large degree of exfoliation observed in PS for the RDP-coated clays. The interfacial activity of these clays was also measured, and we found that the RDP-coated clays segregated to the interfaces of PC/poly(styrene-co-acrylonitrile) blends, while they segregated into the poly(methyl methacrylate) (PMMA) domain of PS/PMMA blends. This morphology was explained in terms of the relative energy advantage in placing the RDP versus the Cloisite clays at the interfaces. Finally, we demonstrated the effects of the relative surface energies of the clays in segregating to the blend air interface when heated to high temperatures. The segregation was shown to affect the composition and mechanical properties of the resulting chars, which in turn could determine their flame retardant response.

1. Introduction

The introduction of a solid particle in a polymer matrix can change the interfacial energy depending on the degree of interaction between polymer chains and the solid surface. As a result, there have been numerous studies, both theoretical and experimental that have studied the effects of nanoparticles on the interfacial properties of binary polymer blend systems. In particular, if the particles have a sufficiently large aspect ratio, compared to the polymer chain diameters, then adsorption could occur leading to the reduction of the free energy of the entire system.[1−12] Theoretically, Lipatov et al. postulated that the energetic factors may be negative if the two polymers are strongly absorbed onto the surfaces of particles, thereby increasing miscibility.[13,14] Experimentally, Si et al.[15] demonstrated this principal using montmorillonite clays functionalized with dimethylhydrogentated tallow, which they showed that the functionalized clays were able to partially compatibilize a large variety of polymer blends and improved their thermal and mechanical properties. They explained their results in terms of the formation of in situ grafts on the clay surfaces, which caused the platelets to segregate to the domain boundaries, thereby reducing the interfacial tension. The adsorption of incompatible polymers to clay surfaces was later explained by Koo et al.[16] to arise from only partial coverage of the platelet surfaces by the functional groups, resulting in the hydrophobic and hydrophilic areas.

*To whom correspondence should be addressed. E-mail: (S.P.) spack@ic.sunysb.edu, parkarrow@hotmail.com; (M.H.R.) mrafailovich@notes.cc.sunysb.edu. Phone: 631-632-2843. Fax: 631-632-5754.

However, this method of compatibilization has several disadvantages. The cation-exchange reactions used to mass produce the clays functionalized with alkyl quaternary ammonium chlorides involve the use of several toxic chemicals[17,18] and the degree of surface coverage is not well-known. The clays modified with quaternary amines are also known to be incompatible with styrenic monomers or the rapidly growing number of different biomass derived polymers, preventing their exfoliation when melt mixed with this rather large class of materials.[19−21] An alternate approach to inducing clay exfoliation is via the adsorption of oligomers into the clay galleries, screening the charges, and allowing for a shear-induced exfoliation. In this case, the requirements are that the oligomers, which are strongly adsorbed to the clay surfaces, interact favorably with mostly nonpolar polymer matrices, and not be easily displaced when compounded in these matrices. These requirements can be contradictory and difficult to satisfy. For example, organic solvents, such as toluene and xylene, have been used to facilitate the exfoliation of clays in nonpolar polymers such as polystyrene or polypropylene.[22−24] Because of the nonpolar nature of the oligomers, this method was only used on ditallow functionalized clays and the solvents used were even less thermally stable than the ditallow surfactants, thereby increasing the thermal instability of the melts.

Here we show that resorcinol bis(diphenyl phosphate) (RDP) can provide a good solution. The chemical structure of RDP is shown in Figure 1, where we can see that it is an oligomeric phosphate ester, which has surfactant properties, since the phenol groups can be considered as nonpolar moieties and phosphoric acids groups can be considered as polar moieties. The oligomers

 Published on Web 05/27/2010

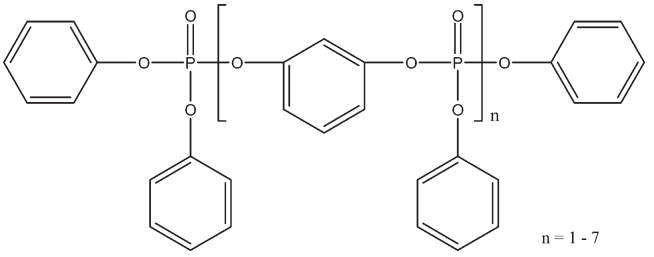

Figure 1. The chemical formula of RDP.

also have the phosphoryl groups that act as a strong hydrogen bond acceptors,[25] and together with the phosphorus groups, which comprise 10.7 wt %, are known to react with polymer residues at high temperatures forming insoluble chars.[26,27] As a result these compounds are often used in flame retardant formulations.

The surfactant properties, together with the fact that these oligomers are stable to temperatures in excess of 300 °C, also make them good candidates for modifying the surface energies of montmorillonite clays. For these clays to exfoliate or be intercalated when blended into a polymer matrix, the strong interactions between the clay platelets must be screened. A common procedure to functionalize the clay surfaces is through charge exchange with ditallow molecules.[17−20] Here, we propose that modification of the clay surfaces can also be achieved by adsorption of RDP molecules. This procedure is far simpler, less toxic, and produces a surfactant coating that is more uniform and thermally stable.

Using complementary characterization techniques, we will show that these clays can be exfoliated, compatibilize blends, and reinforce their mechanical properties to the same degree as the clays functionalized with the alkyl quaternary ammonium chlorides. In addition, we show that these clays can also have the same effects on styrenic polymer matrixes in which the functionalized clays have not been effective. Furthermore, since they are stable to high temperatures, the addition of RDP clays in which there is some degree of exfoliation, allowed the polymers to provide enhanced flame retardant properties. Finally, we will compare the interaction energies between these clays, the ditallow modified clays, and different polymer matrices, where we will try to establish a correlation with the degree of exfoliation, the ability to compatibilize polymer blends, and effectiveness in char formation.

2. Experimental Sections

Materials. Cloisite Na^+, a montmorillonite clays, and Cloisite 20A (C20A) were purchased from Southern Clay Inc. The C20A was modified with a surfactant of dimethyldihydrogenated ammonium chloride. Its surfactant concentration is 95 meq/100 g. Polystyrene and poly(methyl methacrylate) (PMMA) were purchased from Aldrich Sigma and Polysciences. Polycarbonate (PC), average M_w = 23 K, and poly(styrene-co-acrylonitrile) (SAN with 24 wt % AN, known as Luran 358N) were obtained from Amco Plastic Materials Inc. A high-impact polystyrene (HIPS) was received from BASF. The properties of polymers used in this study are tabulated in Table 1. A resorcinol di(phenyl phosphate) (RDP), known as Fyrolflex RDP, was used as a nonhalogen flame retardant (FR) provided by ICL-Supresta Inc. The chemical structure of the RDP is shown in Figure 1.

RDP-Coated MMT-Na^+ (RDP MMT-Na^+) Clays and Nanocomposites Preparation. To obtain the RDP-MMT-Na+ clays, the 20 wt % of RDP was first poured into a 200 mL beaker and continuously stirred on a hot plate at 80 °C, until it melted. MMT-Na+ clays (80 wt %) were then added into the beaker. The mixture was then stirred manually with a 0.5 cm metal rod for 15−20 min or until until the liquid was completely adsorbed into the clay powder. The beaker containing the mixture was removed from the stirring hot plate and was placed in a vacuum oven at 100 °C for 24 h to remove moisture and unabsorbed liquid. The coated clays were then cooled and stored at room temperature prior to blending with polymers. As for the preparation of nanocomposites, a C.W. Brabender with two screw roller blades, Type EPL-V501, was equipped with a direct current drive (type GP100), where the heating chamber was used to mix polymers with nanoclays. The polymeric pellets were first inserted to the chamber at a rotation speed of 20 rpm at high temperatures. The nanoclays, such as C20A and RDP MMT-Na^+ clays, were gradually added into the chamber and mixed at the same rpm for 2 min. The entire melt mixture was further blended at 100 rpm for 15 min under nitrogen gas flow, which prevented degradation of the mixture from heat-induced oxidation. The mixture was allowed to cool to room temperature in the chamber, and then using a hot press, small pieces of the mixture were molded into different shapes required for various experiments. The concentrations of polymer blends containing the clays in this study are summarized in Table 2.

Table 1. Polymers Used in This Study

polymer	MW or grade	manufacturer
polystyrene	280k	Aldrich Sigma
poly(methyl methacrylate) for melt blending	120k	Aldrich Sigma
poly(methyl methacrylate) for spun-casting	75k	Polymer Science
polycarbonate	23k	Mitsubishi Engineering Plastic Corp
poly(styrene-co-acrylonitrile)	Luran 358N	BASF
high-impact polystyrene	5300	BASF
acrylonitrile butadiene styrene (ABS)	Terluran GP-35	BASF
polypropylene	3825WZ	Total Petrochemicals

Table 2. Concentrations of Polymer Blends Used in This Study

polymer blend	concentrations (wt %)
PS/PMMA	70/30
PS/PMMA/RDP MMT-Na^+	70/30/5
PP/PMMA/RDP MMT-Na^+	70/30/5
PC/SAN24	50/50
PC/SAN24/Cloisite 20A	70/30/5
PC/SAN24/RDP MMT-Na^+	70/30/5
PC/SAN24/Cloisite Na^+	70/30/5

Small-Angle X-ray Scattering (*SAXS*). was performed with all samples (2 mm in thickness) to analyze microstructures of layered silicates. Since the silicates were relatively rigid objects compared to the galleries, strong scattering densities could be achieved when the galleries were fully intercalated into the layered silicates. The extended layered silicates with the galleries corresponded to peaks in SAXS, where the scattering vector was only considered one-dimensional to a normal direction of the incident beams because of the large density fluctuations from the rigid silicates in low-scattering regions, which resulted in a circularly symmetric scattering. In the case of organoclays with polymer chains, the peaks could shift toward a lower-scattering vector when the polymer chains were intercalated into the organoclays. Furthermore, when the polymer chains were more intercalated, the organoclays could be eventually delaminated into individual clay platelets, which corresponded to no peaks. Thus, we could determine a degree of organoclays in terms of intercalation with polymer chains. The SAXS was conducted at a beamline X10A at National Synchrotron Light Source (NSLS) at Brookhaven National Laboratory. The wavelength used in the beam was 1.09 Å. The q range was from 0.03 to 0.58 $Å^{-1}$. The distance between the samples and the detector was 81.20 cm.

Transmission Electron Microscopy (*TEM*). TEM was conducted with the cross sections from the nanocomposites. The thickness of the cross sections was 70−80 nm, which were cut by a Reichert-Jung Ultracut E Ultramicrotome and then were floated on deionized (DI) water surfaces. Later, a few cross sections were

placed on a coated copper mesh grid. The sections were directly viewed from a FEI Tecnai12 BioTwinG^2 TEM at 80 KV and digital images were obtained from an AMT XR-60 CCD digital camera system. The RDP agents in the polymer matrixes were verified by an energy dispersive X-ray spectroscopy (EDXS) in the SEM (LEO-1550) with a Schottky field-emission gun where the surfaces of RDP nanoclays were coated with a few micrometers of gold to make the specimens conduct.

Scanning Transmission X-ray Microscopy (*STXM*). STXM, which was located at X-1A beamline at National Synchrotron Light Source (NSLS) at Brookhaven National Laboratory (BNL), was used to determine the chemical composition of polymer blends. The forced X-ray beam was confined into a 55 nm Rayleigh resolution spot using a Fresnel zone plate.[28] The beam was able to scan the cross sections with 70−80 nm thickness. The cross sections were cut from the bulk compounds using a Reichert-Jung Ultracut E microtome and then they were lifted on coated copper mesh TEM grids on DI water surfaces. The scanning process performed outbound photo energies of components and the zone plate to the cross-section distance. Hence, the images and spectra were collected at the same time. The images at specific photon energies were representative to strong absorption of one of phases, where dark phases in the images corresponded to high energy absorption and light phases were obtained at low energy absorption.[29]

Atomic Force Microscope (*AFM*). The sample morphology was imaged with a VEECO/DI-3000 scanning force microscope using a silicon nitrate tip in the contact mode. Since the clays are harder than the surrounding obtained substrates, they were easily imaged in the lateral force mode. Furthermore, the Langmuir clay films were also imaged, and from the topography images we obtained the height of the platelets and the height of the RDP layer. Here as well, there was substantial friction contrast between RDP and the clay surface, which allowed us to determine the degree of coverage, which was nearly complete. Si(111) substrates were prepared by a modified Shiraki technique, where small pieces of the Si substrates (0.5 × 0.5 in.) were immersed in a mixture of $H_2O/H_2O_2/H_2SO_4$ (3:1:1 vol) for 15 min at 100 °C. After that, the Si substrates were washed with DI water and then etched in HF/H_2O (1:4 vol) for 15 s at room temperature. The formation of monolayer clays were prepared by Langmuir−Blodgett (LB) technique. In the previous study,[16] 20 mN/m was used as a surface pressure (π) to obtain a monolayer of the clays on the etched Si substrates. The polymer solutions were spun-cast on glass substrates. The thin films (~100 nm) from the glass substrates were floated on the surfaces of DI water and then the thin films were lift on the Si substrates with monolayer clays.

Contact Angle Measurements. The polymer/clay bilayer samples were placed in a vacuum oven and annealed for up to 48 h at $T = 180$ °C and $P = 10^{-3}$ Torr. The morphology of the films was then studied using atomic force microscopy, as described in ref 30. In the case of the bilayers, where dewetting occurred, the contact angle between the droplets formed by the polymer film and the clay surface were directly measured using the VEECO/DI contact angle software. Each measurement represents the average measurements of 10 droplets per sample. The values were also checked from the simple formula where $\tan \zeta = h/r$ where h is the height of the droplet and r is the radius of the base.

Instrumented Indentation. Instrumented indentation was performed using a nanoindenter (Micro Materials NanoTest) with a 5 μm radius of curvature diamond cone indenter. Depth-controlled indentations were performed with the maximum depth set to 2 μm. Char samples were mounted with an epoxy adhesive to aluminum sample holders for testing. Because of the large variation in char topology, regions were identified using a light microscope, which were flat and free of pores. Load−displacement data was obtained using a constant loading and unloading rate of 0.1 mN/s. The typical maximum loads reached were on the order of 9−12 mN. A 5 s hold segment was taken at the maximum displacement before unloading to take into account

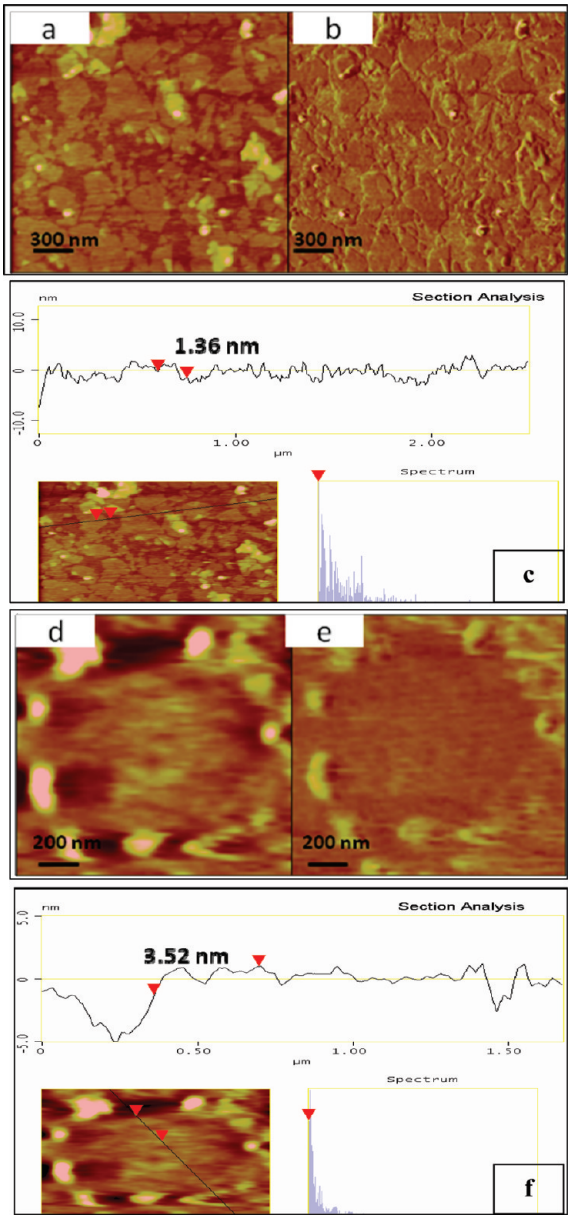

Figure 2. AFM images of uncoated MMT-Na$^+$. (a) Height and (b) friction, and (c) cross-section of uncoated MMT-Na$^+$. AFM images of RDP-coated MMT-Na$^+$ (d) Height and (e) friction and (f) cross-section of RDP-coated MMT-Na$^+$.

creep effects. On each sample, three identical indentations were performed with a minimum spacing interval of 60 μm between successive indents to ensure no interaction between residual plastic deformations. To determine elastic modulus of the char material, the slope (S) of the initial unloading data in conjunction with the spherical contact area is used in the conventional Oliver and Pharr method to determine a reduced modulus.[31] The contact radius as a function of the plastic depth (h_p) of the char is given as

$$a = \sqrt{2Rh_p - h_p^2}$$

where R is the radius of the indenter (5 μm) and h_p is the average of the residual and maximum depth of the indentation. The reduced modulus (E_r) can be written as

$$E_r = \frac{3}{4}\frac{S}{(2Rh_p - h_p^2)^{1/2}}$$

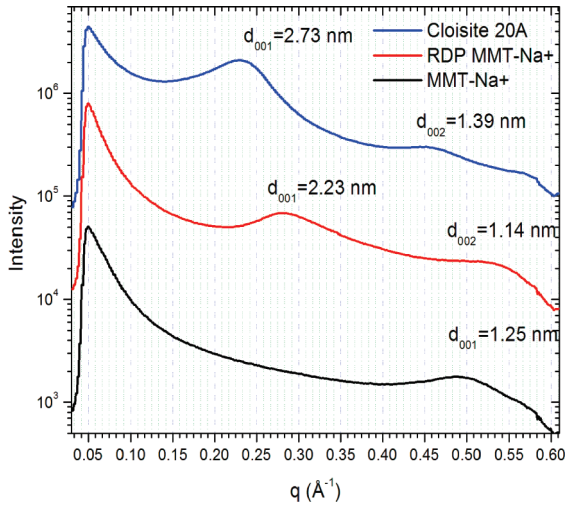

Figure 3. SAXS spectra of nanoclays.

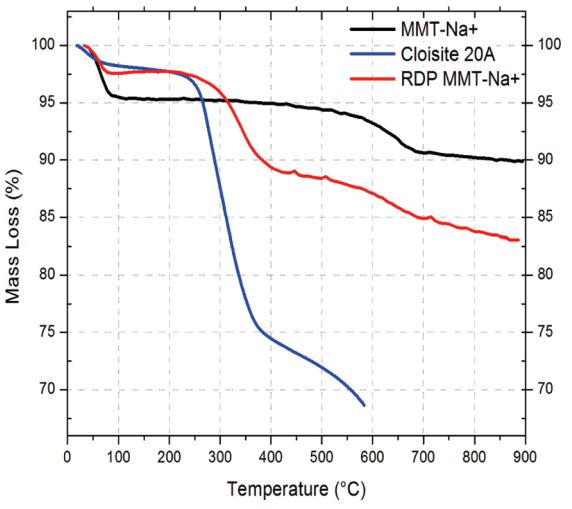

Figure 4. TGA curves of nanoclays.

where S is the slope of the unloading curve, and E_r is represented by

$$\frac{1}{E_r} = \frac{1-\nu_s^2}{E_s} + \frac{1-\nu_i^2}{E_i}$$

With knowledge of the elastic modulus and Poisson's ratio of the indenter tip (E_i = 1141 GPa, and ν_i = 0.07), it is possible to determine the elastic modulus of the chars (E_s) from the reduced modulus, assuming a char Poisson ratio of ν_s = 0.5, typical for incompressible materials. Hardness (H) of the chars was calculated by the ratio of the maximum applied load (P_{max}) divided by the contact area ($A = \pi a^2$). The reported material properties of the char surfaces were averaged over three discrete indentations.

Mechanical and Thermal Analysis and FT-IR Spectroscopy. Elastic modulus and tan δ of the samples were performed using a Mettler Toledo DMA/SDT 861e in the single cantilever mode. The samples were molded into bars of dimension 10 mm × 10 mm × 2 mm and then were measured as a function of temperature. The range of temperatures were from room temperature to 180 °C at a rate of 2 °C/min with a frequency of 1 Hz. Thermogravimetric analysis (TGA) was conducted at a Mettler-Toledo 2000 analyzer to compare the RDP MMT-Na^+ clays with the C20A clays in terms of the rate of mass loss of the clays in the N_2. The mass of samples (8−10 mg) were placed into an aluminum crucible. The crucible with the mass was put on the small dish at the furnace in the TGA and then the temperature was raised from 30 to 800 °C at a rate of 10 °C/min. The FT-IR spectra of RDP and clays were obtained from MAGNA-IR 760 spectrometer made by Nicolet. The samples were first mixed with KBr powder and then were hydraulic-pressed to a pellet for FT-IR spectroscopy.

3. Results and Discussion

3.1. RDP-Coated Nanoclays. *Morphology and X-ray Scattering*. In Figure 2, we show the scanning force microscopy images of RDP-coated MMT-Na+ and uncoated MMT-Na+ clay monlayers that were produced by lifting from the air−water interface onto a Si wafer. In the figure, we see the distinct outline of the platelets both in height and lateral friction scans of the unmodified. The outline of the platelets is more difficult to observe on the coated samples. The surfaces of both types of clays are relatively smooth topographically. This indicates that the RDP coating is fairly uniform. In Figure 2c,f, we also show a cross sectional scan of the coated and uncoated platelets, where we can see that the uncoated ones are 1.36 nm in height while the coated ones are 3.52 nm in height. We could then estimate that the height of RDP surfactant layer coating the

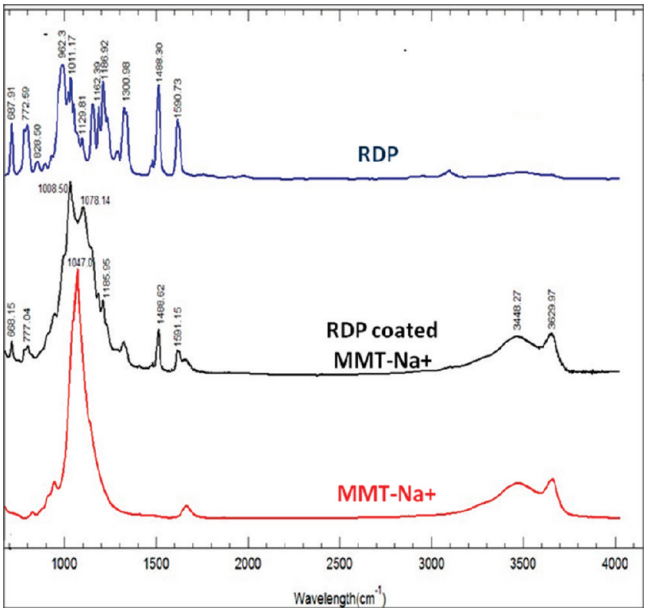

Figure 5. FTIR spectra of nanoclays. RDP, blue line; RDP-coated MMT-Na^+, black line; and MMT Na^+, red line.

clay surfaces was about 2.2 nm. In Figure 3, we show SAXS spectra of the coated and uncoated clays. From the figure we can identify the characteristic peak in the unmodified clays, at q = 0.50 $Å^{-1}$, which is in agreement with previously reported results and corresponds to d = 1.25 nm the [001] direction. A large shift in the characteristics peaks is observed for the RDP clays, where the [001] peak is observed at q = 0.282 $Å^{-1}$ and even the secondary [002] peak is observed at q = 1.14 nm. Using the $d = 2\pi/q$, and substituting q = 0.282 $Å^{-1}$, we find that the interlayer spacing has increased to 2.23 nm as in the direction of [001], which is in excellent agreement with the value measured on the scanning force microscope images. For comparison, we also show the X-ray scattering data obtained from a Cloisite 20A monolayer lifted by the same LB technique from the air/water interface. Here the primary peak is seen to shift to q = 0.2319 $Å^{-1}$, which corresponds to an interlayer spacing d = 2.7 nm in the [001] direction, which is in good agreement with previously reported data[16] and somewhat thicker than the RDP layer.

Thermal Stability. TGA analysis was performed. From Figure 4, we can see that approximately 5% of mass loss on

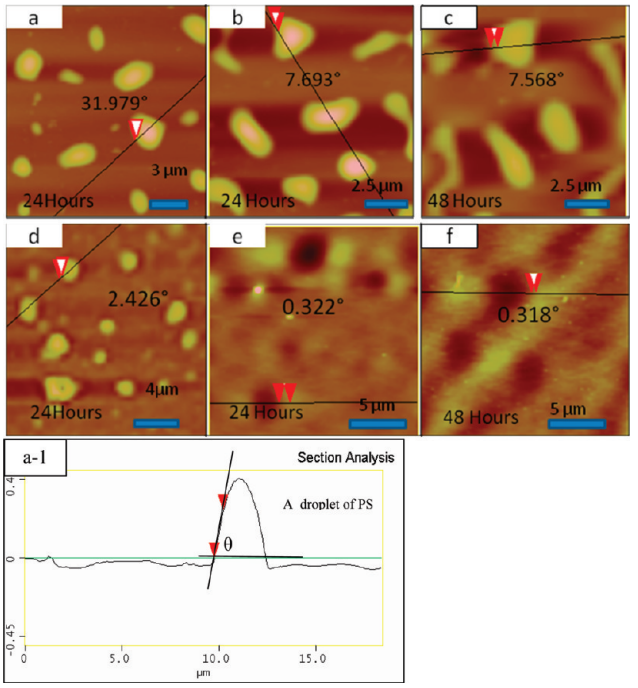

Figure 6. The contact angles on polymer thin films on clays. (a) PS/Cloisite 20A and (b) PS/RDP MMT-Na^+ after 24 h annealing, and (c) PS/RDP MMT-Na^+ after 48 h annealing. (d) PMMA/Cloisite 20A and (e) PMMA/RDP MMT-Na^+ after 24 h annealing, and (f) PMMA/RDP MMT-Na^+ after 48 h annealing. (a-1) A cross scan of PS/Cloisite 20A.

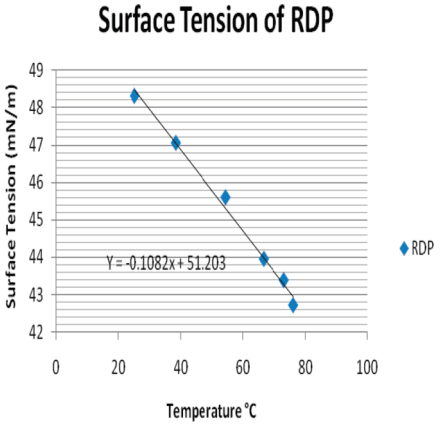

Figure 7. The surface tensions of RDP as a function of temperature.

unmodified MMT-Na^+ clays occurs at around 100 °C due to the vaporizations of moiety molecules unbounded onto the clays. However, in the case of Cloisite 20A, only 2.5% of mass loss is obtained before the major decomposition undergoes around 250 °C. This mass loss could be indicative that the ditallow molecules are firmly confined into the clays, which could lead to the strong interactions between polymer chains and the surfactants in the direct intercalation of polymer melt.[32,33] On the other hand, the RDP-coated MMT-Na^+ clays also have the small mass loss before the clays start to decompose at round 300 °C. The higher decomposition temperature could be mainly contributed to the decomposition of RDP, which degrades at 288 °C (about 5 wt % loss).[34] However, the extra increase of decomposition temperature (about 12 °C) may result from a synergic effect, where the RDP-coated clays could be more stable on higher temperatures. The synergic effect on the presence of RDP on the clay surfaces

Table 3. Polymer Surface and Interfacial Tensions

polymer	surface tension (mN/m)	interfacial tension $\gamma_{Polymer/Polymer}$ (mN/m)	interfacial tension $\gamma_{RDP/Polymer}$ (mN/m)
PS	29.2		2.75
PMMA	28.9		2.8
PS/PMMA		1.2	
PP/PMMA		9	
PC	29.1		0.5 (if $S = 0$)
SAN24	35.3		
PC/SAN24		2.8	

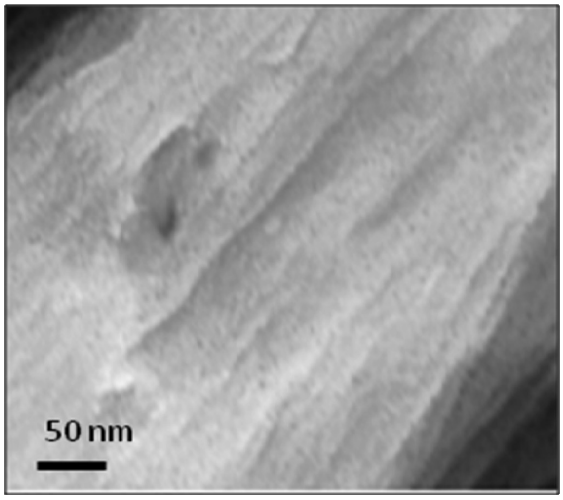

Figure 8. The TEM image of a cross-section from PMMA/RDP MMT-Na^+ nanocomposite.

could be contributed to the spectra of RDP-coated MMT-Na^+ in FT-IR as well. From Figure 5, we can see that the unmodified clays show typical characteristic absorption bands, 1047, 3448.27, and 3629.97 cm^{-1}, which correspond to one of Si−O stretching regions, O−H stretching regions, respectively. In particular, the Si−O stretching band separates into the two peaks, 1008 and 1078 cm^{-1}, when the RDP is incorporated. Yan and Cole found that peak II (~1080 cm^{-1}), which is the out-of plane mode, became visible clearly as the content of water or compatiblizer increased into the clay interlayers.[35,36] Thus, it is clearly indicative that the RDP oligomers are intercalated into the clay galleries. Furthermore, the RDP IR spectrum shows that there are the phosphorus−oxygen double bond stretching (P═O) at ~1300 cm^{-1} and the phosphorus−oxygen single bond stretching (P−O) at ~960 cm^{-1}. The absorption band of the P═O still appears at the same position in the RDP clays spectrum. However, the P−O absorption band might be shift to at 1008 cm^{-1}, which may result from the presence with hydrogen bonding. Since the phoshoryl group (P═O) in the RDP oligomers are well-known as a strong acceptors for hydrogen bonding,[25] the RDP oligomergs would be self-assembled in the clay galleries, which could be biocompatible to biomass polymers, such as starch, which will be presented in the following report.

Contact-Angle Measurements. To determine the relative affinity for the polymers, the RDP-coated clays or the Cloisite 20A clays, films of spun cast PS or PMMA were floated on top of the LB monolayers and annealed for times up to 48 h at $T = 180$ °C. The results are shown in Figure 6, where we also show in figure 6a-1 a cross sectional scan indicating where the contact angle was measured. At this temperature, the surface tensions of PS and PMMA are nearly equal ($\gamma \sim$ 29 mN/m)[37] and hence differences in the contact angle are mostly due to differences in the interfacial energy between

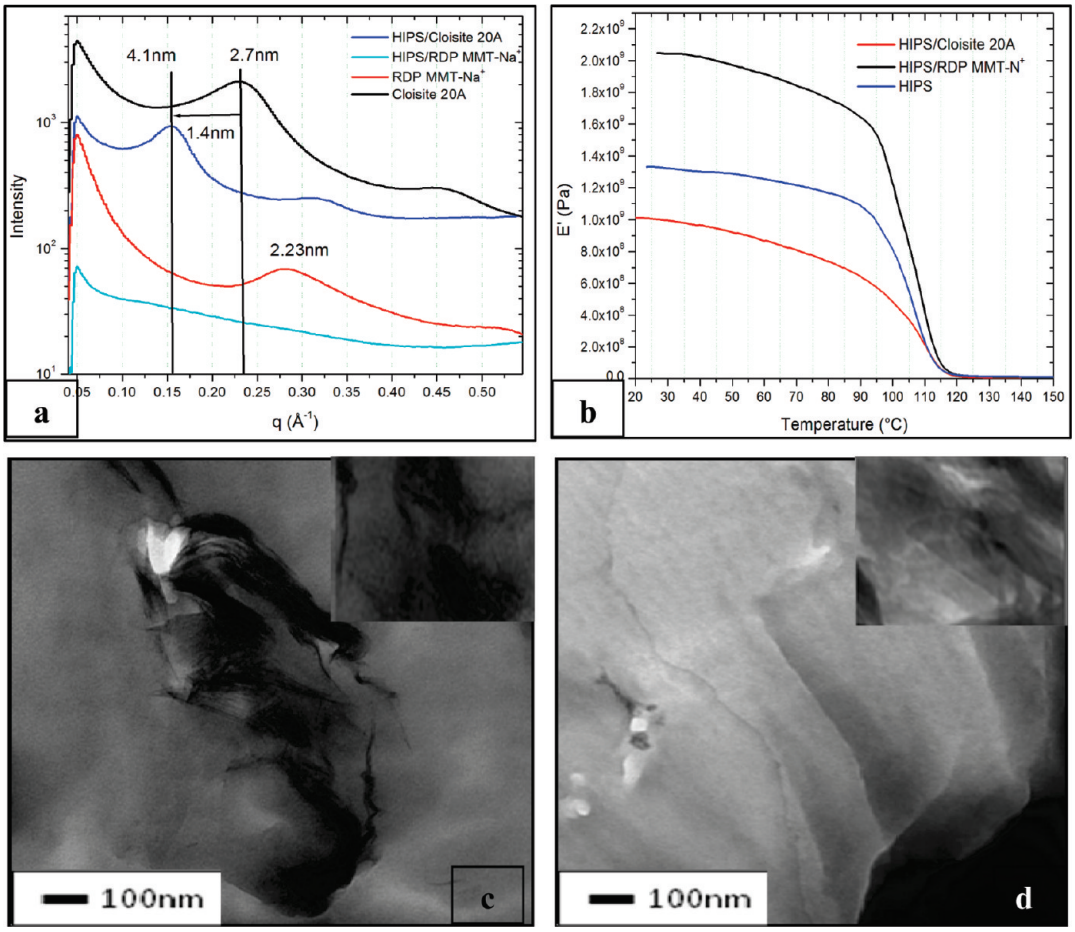

Figure 9. (a) SAXS spectra of HIPS/nanoclays nanocomposites, (b) storage modulus and tan δ of HIPS/RDP clays nanocomposite (the inserted image). TEM images of HIPS/nanoclays composites: (c) HIPS/Cloisite 20A, highly intercalated; and (d) HIPS/RDP MMT-Na^+, exfoliated.

the polymers and the surface. Since the surfactant layers on clays are thin and strongly adsorbed, our system can be followed by Young's law rather than a Neuman construction.[38] We can assume that the observed angles correspond to the Young's contact angle

$$\gamma_A = \gamma_B \cos\theta + \gamma_{A/B} \quad (1)$$

where γ_A and γ_B are the surface tension of the A and B phases, and $\gamma_{A/B}$ is the interfacial tension between the A and B phases. From the figure, we can see that the contact angle for PS on RDP covered clays reaches an equilibrium value of 7.7° after 24 h of annealing and does not change significantly after additional annealing of another 24 h. The PMMA film, on the other hand, appears to wet on the RDP-coated clay surfaces and the holes initially formed upon deposition of the PMMA film do not seem to increase in diameter, nor do droplets form on the surface after 48 h of annealing.

To determine the interfacial tension between the RDP-coated clays and the homopolymers, we first had to find the surface energy of RDP as a function of temperature. This was performed using the Wilhelmy plate method on a volume of 78 cm^3 of RDP heated from ambient to 80 °C. The data are shown in Figure 7, where we derive the equation, $y = -0.1082x + 51.203$, where x is temperature and y is a surface tension at a temperature, and from which we can extrapolate a value of 31.7 mN/m at 180 °C. Substituting this value for γ_A in eq 1 we find that $\gamma_{A/B}$ is 2.75 and 2.8 mN/m for RDP with PS and PMMA, respectively, which is shown in Table 3.

We can now determine whether PS or PMMA will wet the RDP-coated clays at $T = 180$ °C or the conditions used in melt mixing the nanocomposites. The spreading coefficient S is given by

$$S = \gamma_{RDP} - \gamma_{Polymer} - \gamma_{RDP/Polymer} \quad (2)$$

where wetting occurs when $S > 0$. Hence for PS we obtain $S = -0.25 < 0$ and for PMMA $S = 0 \sim 0$, which is consistent with the observation that PMMA completely wets the RDP-coated clay surface, whereas PS does not. Therefore, the RDP-coated clays are expected to exfoliate in a PMMA matrix to expose more interfaces. This observation is confirmed in the TEM image shown in Figure 8. In the case of PS, the spreading coefficient is only slightly negative, and the some exfoliation can occur when shear is applied. TEM images of RDP clay nanocomposites with HIPS are shown in Figure 9, where a high degree of exfoliation is observed.

In Figure 6, we show the contact angles obtained on Cloisite 20A monolayers. In this case, we find that the angle of PS is rather high, or 32°, indicating that a large unfavorable interfacial tension exists. This is in good agreement with the known lack of exfoliations of the Cloisite 20A in PS matrices. The angle with PMMA, on the other hand, is only 2°, which is consistent with the known ability of PMMA matrices to exfoliation of the Cloisite clays under shear.

3.2. Nanocomposites. *Homopolymers.* To examine the degree of exfoliation of the RDP clays in thermoplastic polymers, such as a HIPS, poly(acrylonitrile butadiene styrene) (ABS), and polypropylene (PP), we performed SAXS experiments and compared

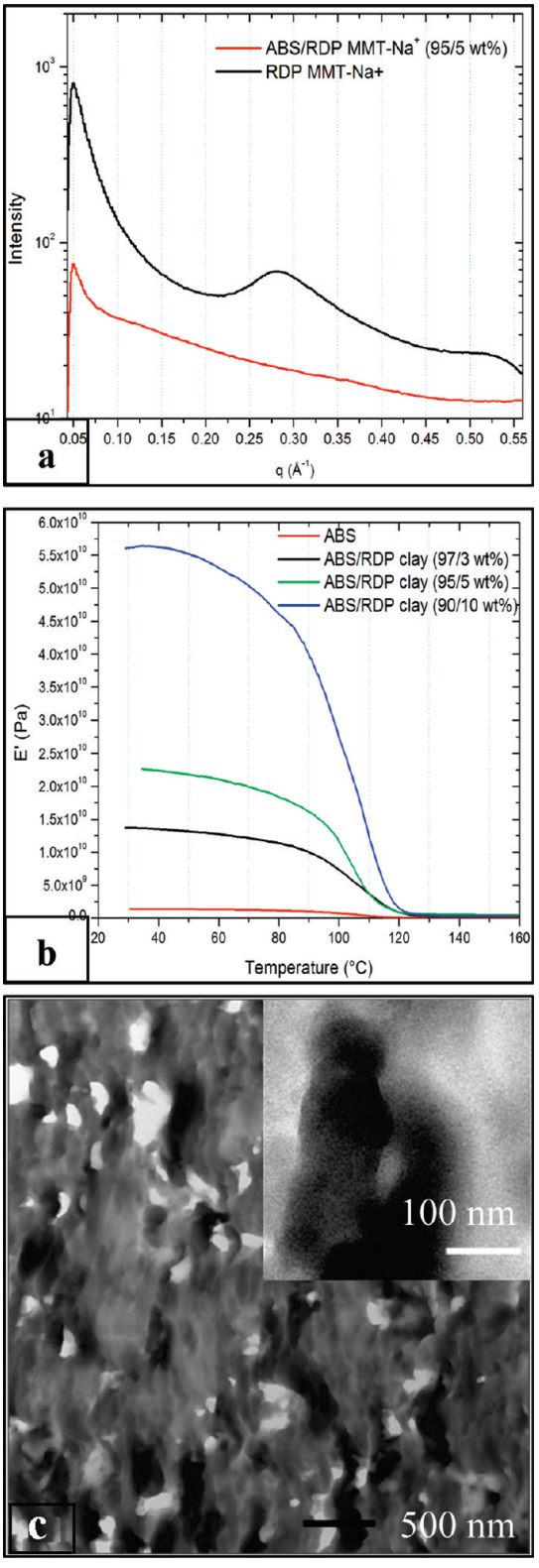

Figure 10. ABS/RDP MMT-Na^+ nanocomposites: (a) SAXS spectra, (b) storage modulus, (c) TEM images.

the results with TEM images for polymers that could be cross sectioned at ambient temperatures.

From Figure 9a, we show the SAXS data for HIPS nanocomposistes with either 5% Cloisite 20A or RDP-coated clays, and we plot the data for just the clays as a reference point. From the figure, we see that in the nanocomposite with Cloisite 20A the [001] as well as the [002] scattering peaks are

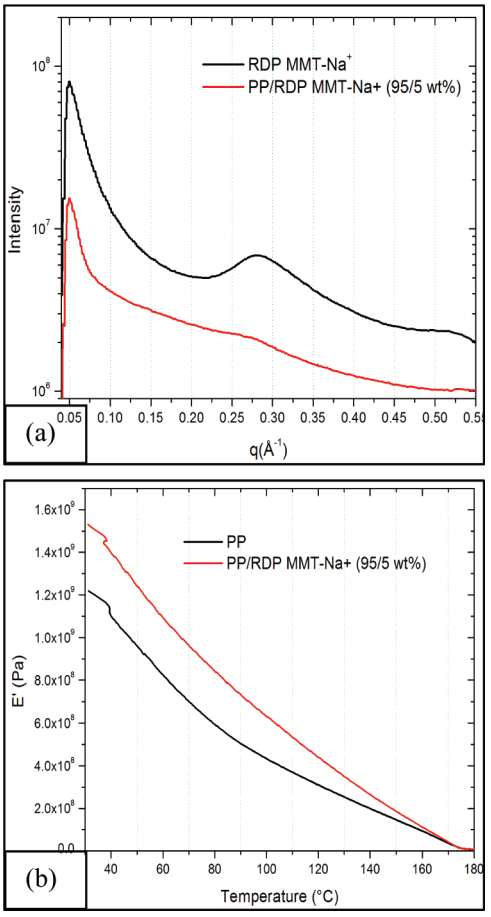

Figure 11. PP/RDP MMT-Na^+ nanocomposites: (a) SAXS spectra, (b) storage modulus.

clearly visible and are of comparable intensity to the peaks of the pure clays. From the shifts in the peaks, we find that the interlayer spacing has increased further to 4.1 nm, which indicates that most of the clay are intercalated, rather than exfoliated, with a layer that is approximately 1.4 nm thick of polymer. In contrast, for the HIPS/RDP clays nanocomposite, no scattering peaks are observed, which is consistent with most of the clays being exfoliated. This is further confirmed by the TEM micrographs shown in Figure 9c,d. In Figure 9c, we show a typical cross sectional image of the HIPS/Cloisite 20A nanocomposite, where we see large tactoid-like structures, where the clay platelets are intercalated with polymers. From the inserted TEM image we can estimate the mean distance between platelets to be 4.2 nm, which is in a good agreement with the scattering data. In contrast, from Figure 9d we can see a typical cross sectional image of the HIPS/RDP MMT-NA^+ nanocompoiste. Here mostly individual platelets are seen, which would not produce diffraction peaks, confirming the exfoliated nature. These results are consistent with the contact angle measurements shown previously, where the interfacial tension between PS and RDP-coated clays was found to be much smaller than that with the ditallow coated clays, facilitating the exfoliation of the RDP-coated clays during shear mixing.

Exfoliation is also more efficient at modifying the mechanical properties than intercalation. This is also demonstrated in Figure 9b where we plot the dynamic modulus and tan delta of HIPS/clay nanocomposites, obtained from DMA measurements as a function of temperature. From the figure, we see that in both cases the addition of clays does not affect on the glass transition temperature, Tg, which remains as

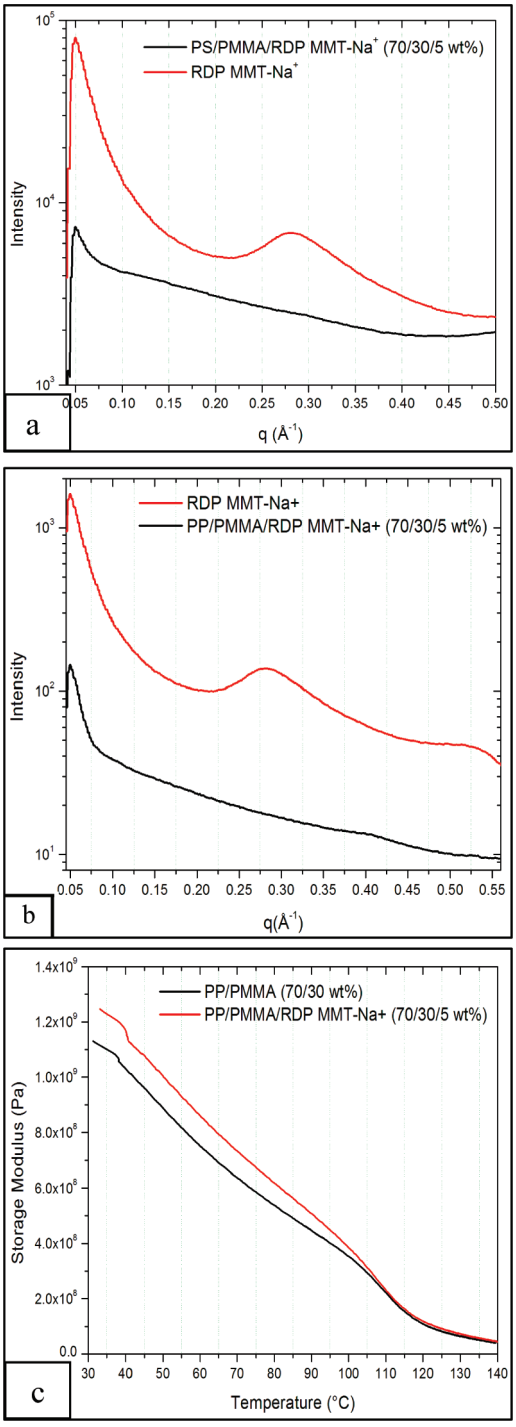

Figure 12. SAXS spectra: (a) PS/PMMA/RDP MMT-Na^+ (70/30/5 wt %), (b) PP/PMMA/RDP MMT-Na^+ (70/30/5 wt %) nanocomposites, and (c) storage modulus of PP/PMMA/RDP MMT-Na^+ (70/30/5 wt %).

same as the HIPS homopolymer. On the other hand, we see that the addition of RDP clays increases the modulus by nearly a factor of 2 for $T < Tg$, whereas the addition of Cloiste 20A slightly decreases on the modulus, which is consistent with the poor mixing of the Cloisite clays with the polymers.

In Figure 10, we show the SAXS data obtained for another nanocomposite with styrene groups, ABS with 5 wt % RDP clays. Here we also find that the clays diffraction peaks are not observed, while the TEM cross-sectional image indicates a good exfoliation. The storage modulus of the nanocomposites with RDP clays increases by nearly an order of magnitude

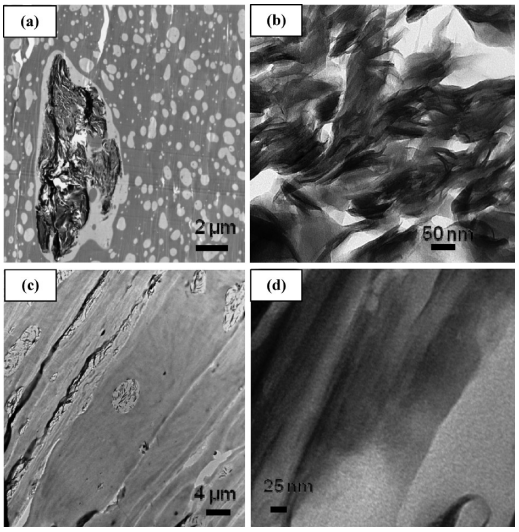

Figure 13. TEM images: (a,b) PS/PMMA (70/30 wt %) and (c,d) PP/PMMA (70/30 wt %) with 5% the RDP MMT-Na^+ clays.

compared to that of homopolymer, which could mainly result from the fully exfoliation of the clays. Since the increase in the rubber fraction did not seem to affect the degree of exfoliation, we also attempted to blend the RDP clays with PP homopolymer, another polymer in which numerous authors have reported difficulties with Cloisite 20A. The SAXS data is shown in Figure 11a, where we find only a small trace peak at the position of the RDP-clays [001] indicating most of the clays are exfoliated. This is further confirmed by the DMA data shown in Figure 11b, where we see that the storage modulus of the RDP clays nanocomposite is higher than that of the PP homopolymer up to the melting temperature.

Polymer Blends

Blends of PMMA with Either PS or PP. In Figure 12, we show the SAXS data from blend samples composed of 30% PMMA with either 70% PS (Figure 12a) or 70% PP (Figure 12b) and 5% RDP-MMT-Na^+ clays. The scattering peaks of the pure RDP-coated clays are also plotted for comparison. In each case, we see no remnant of the clay peaks indicating that a full exfoliation has occurred. In the previous paper,[6] we claimed the partial compatibilization of the PMMA/PS blend when Cloisite 20A was added, yet the SAXS data indicated the presence of the clay peaks intercalated with the polymers. High- and low-magnification TEM images of both of these blends are shown in Figure 13a,b. From the figures, we conclude that the absence of the clay peaks in the SAXS data do not necessarily correlate with compatibilization. In the case of the PS/PMMA blend, the clays are entirely segregated within the PMMA phase, where they appear as large intercalated tactoids. In contrast to the TEM images of ref 15, no platelets are observed at the polymer phase interfaces, and hence no effect of the RDP-coated clays can be seen on the compatibilization of this blend. In the case of the PMMA/PP blend, most of the clays are still in the PMMA domains, where they can also exfoliate, as they do in the homopolymer. In contrast to the TEM images for the blend with PS, some of the platelets are seen to be adsorbed onto the phase interfaces shown in Figure 13c,d, which could lead to an increase of the dynamic modulus overall temperatures compared to the blend without the RDP-coated clay. It is shown in Figure 12c.

From the contact angle data shown previously, we have demonstrated that PMMA wets the surfaces of the RDP-coated

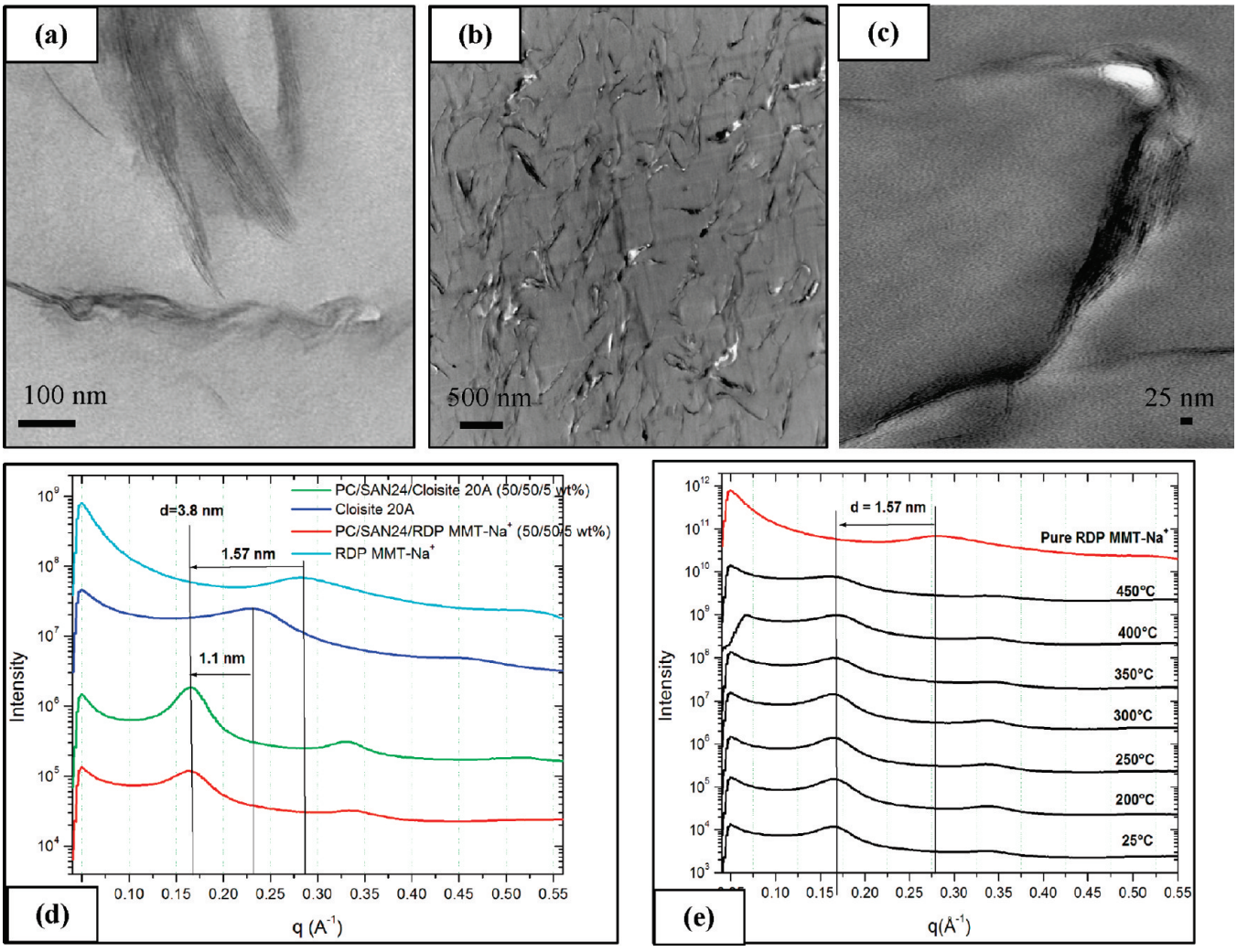

Figure 14. TEM images: (a) PC/SAN24/Cloisite 20A (50/50/5 wt %), (b) PC/SAN24/RDP MMT-Na^+ (50/50/5 wt %) - low magnification, and (c) PC/SAN24/RDP MMT-Na^+ (50/50/5 wt %) - high magnification. SAXS spectra: (d) PC/SAN24/RDP MMT-Na^+ and PC/SAN24/Cloisite 20A, and (e) PC/SAN24/RDP MMT-Na^+ as a function of temperature.

clays, while PS dewets the surfaces. During the melt-mixing process at high temperatures, the PMMA chains will preferentially be adsorbed onto the RDP-coated clay surfaces, forming in situ grafts composed almost entirely of PMMA chains. Hence the RDP-coated clays will segregate exclusively in the PMMA domains, and no reduction of the overall energy of the system occurs when these platelets are placed at the phase interfaces. Furthermore, the interfacial energy between PS and PMMA, $\gamma = 1.2$ mN/m at 180 °C,[37,39] is lower than either of the interfacial tensions (Table 3); between either of the blend polymers and RDP, no energetic advantage is obtained through segregation at the interface. Hence the RDP-coated clays are massively segregated in the PMMA phase, where their interfacial energy is minimized, and no change in the blend compatibility occurs.

In Figure 13c,d, we show TEM data corresponding to a PP/PMMA blend. In this case, some compatibilization is observed in the lower-magnification images, while some clays at the blend interfaces are observed in the higher magnification image. Since the interfacial tension between PP/PMMA has been reported, $\gamma_{int} = 4.5$ mN/m[40] at 240 °C and $\gamma_{int} = 7.50$ mN/m[41] at 200 °C, we could extrapolate the interfacial tension of blend as $\gamma_{int} \sim 9$ mN/m at 180 °C or significantly higher than that between RDP and PMMA, $\gamma_{int} \sim 2.8$ mN/m. As we have shown that the RDP clays exfoliate in PP as well, we can estimate that the interfacial tension with PP would be comparable to that with PMMA, and hence placing the RDP clays at the polymer interfaces can reduce the overall energy of the system and result in partial compatibilization. Therefore, even though the spreading parameter is positive for this system, there is still a relative reduction in the overall energy of the system when the clays are placed at the interface, hence increasing the degree of compatibility.

PC/SAN24 Blend. From Figure 14a−c, we can see TEM images of cross-section samples of a PC/SAN24 blend. In both cases, we find either 5% Cloisite 20A or RDP-coated clays are fairly intercalated rather than exfoliated. This observation is consistent with the SAXS data obtained from these samples, shown in Figure 14d, where peaks are observed corresponding to either Cloisite 20A or RDP-coated clays, with large intergallery spacings corresponding to an intercalated system. In addition, the intercalation of RDP-coated clays could be stable up to 450 °C in which the peaks still remain at the high temperature in Figure 14e.

We also confirmed that the addition of the RDP clays improved the compatibility of the polymer blend using the STXM technique. In Figure 15, we show a STXM images obtained from a symmetric PC/SAN24 blend mixed without clays and either with 5% Cloisite Na^+ or 5% RDP clays,

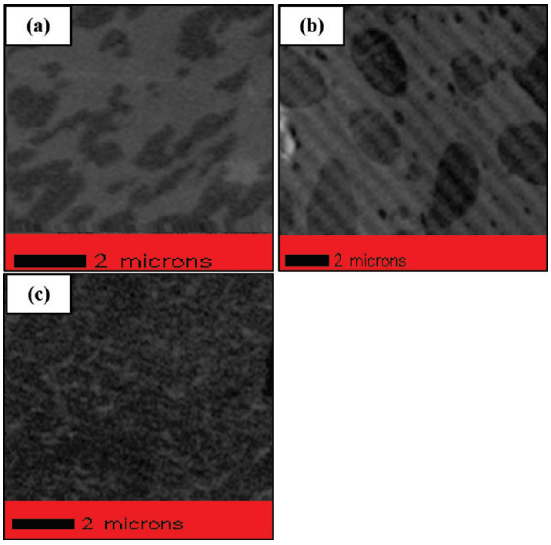

Figure 15. STXM images: (a) PC/SAN24 (50/50 wt %), (b) PC/SAN24/Cloisite Na^+ (50/50/5 wt %), and (c) PC/SAN24/RDP MMT-Na^+ (50/50/5 wt %). The images were taken at 286.70 eV. (Dark regions are the rich SAN 24 phases.)

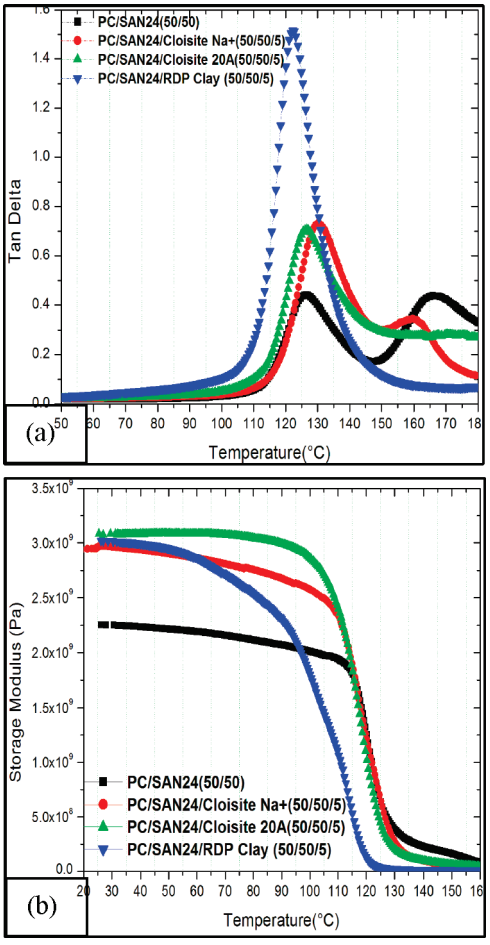

Figure 16. PC/SAN24 nanocomposites: (a) Tan δ and (b) storage modulus.

which were cross sectioned after removal from the Brabender. In the figure, PC and SAN24 correspond to the light and dark areas, respectively. From Figure 15a, we can see that in the absence of clays the domains are well separated from each other. The addition of Cloisite Na^+ clays further enhances the

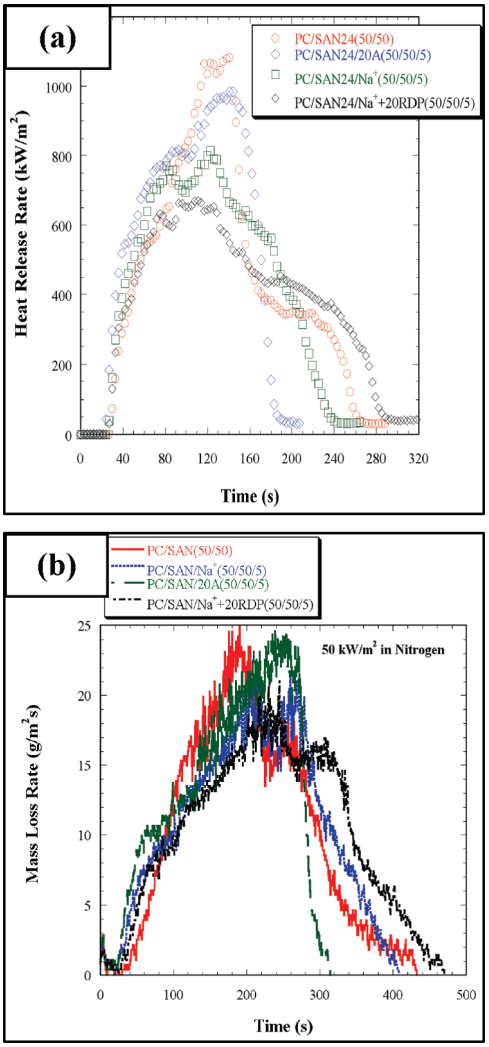

Figure 17. (a) HRR and (b) MLR of PC/SAN24/Clays nanocomposites in N_2.

Table 4. Yield of Carbonaceous Chars for PC/SAN24 with Clays in Air

nanocomposite	carbonaceous chars yield
PC/SAN24	19%
PC/SAN24/MMT-Na+	10%
PC/SAN24/Cloisite 20A	10%
PC/SAN24/RDP-coated MMT-Na+	11%

Table 5. Yield of Carbonaceous Chars for PC/SAN24 with Clays in Nitrogen

nanocomposite	carbonaceous chars yield
PC/SAN24/MMT-Na+	8%
PC/SAN24/Cloisite 20A	8%
PC/SAN24/RDP MMT-Na+	3%

phase segregation, probably due to segregation of the clays in the PC phase (Figure 15b). However, the addition of 5% RDP-coated clays dramatically changes in the morphology of the blend, where the domains become bicontinuous and smaller than the resolution of the image (50 nm), which is shown in Figure 15c. This phase segregation can be explained by minimizing the interfacial energy of the blend. To quantify the energy, we can apply the values of surface tension for PC and SAN24, reported in literatures. We found that the interfacial tension for PC/SAN24 blend was ~2.8 mN/m,[42,43] and

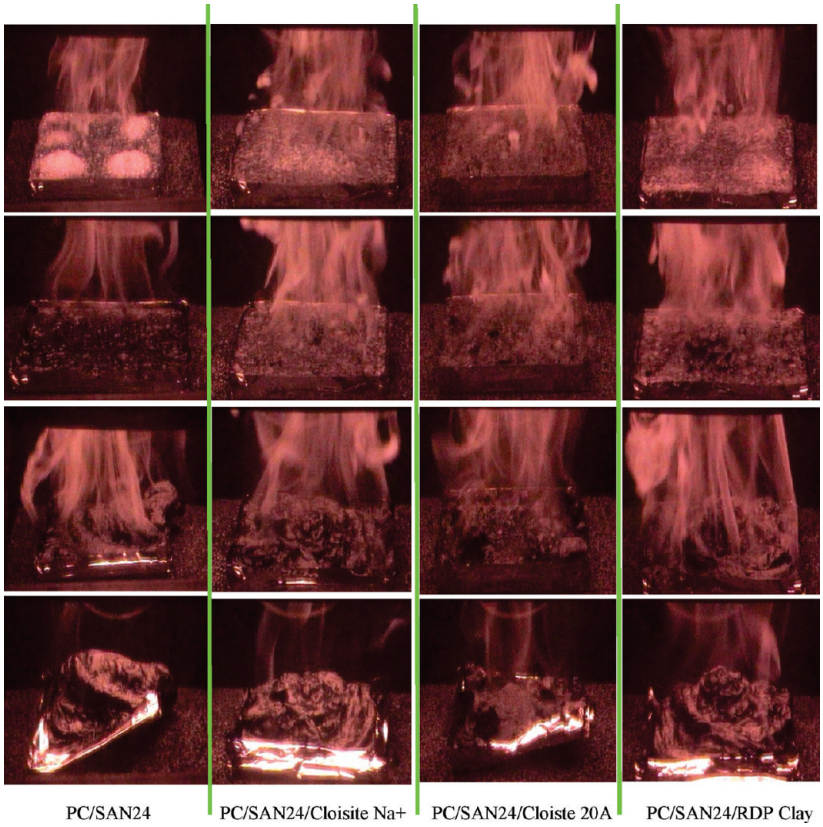

Figure 18. A selected video images at 30, 100, 230, and 300 s from the gasification tests: PC/SAN24 (50/50 wt %), the first column; PC/SAN24/Cloisite Na^+ (50/50/5 wt %), the second column; PC/SAN24/Cloisite 20A (50/50/5 wt %), the third column; and PC/SAN24/RDP MMT-Na^+ (50/50/5 wt %), the fourth column.

the surface tension for PC at 200 °C was 29.1 mN/m.[44] Since we know the temperature dependence of the surface tension for the RDP oligomers, we can calculate a value of the surface tension of RDP is 29.6 mN/m at 200 °C. Hence we can see that the spreading coefficient S_{PC} on RDP clay surfaces almost is zero without adding the interfacial tension between PC/RDP. If $S_{PC} = 0$, $\gamma_{RDP/PC}$ is 0.5 mN/m. Although values of the surface tension for SAN24 at 180 °C is not available, the surface tension for SAN24 can be calculated using the temperature dependence of polystyrene ($-d\gamma/dt = 0.072$);[37,44] γ_{SAN24} is 35.3 mN/m at 200 °C. As we can see, the spreading coefficient S_{SAN24} on RDP clay surfaces is already negative. Thus, when the SAN24 polymer melts dewets a value of $\gamma_{RDP/SAN24}$ would be higher than that of $\gamma_{PC/SAN24}$. Therefore, the maximization of reducing the interfacial energy could occur when all of RDP-coated clays segregate at the interfaces, while increasing the compatibility.

Furthermore, we could also confirm the blend on the compatibility by obtaining a single Tg. From Figure 16a, we can see that the blend has two distinct glass transition temperatures in which one is about 127 °C for SAN24 and the other is about 170 °C for PC. When the Cloisite Na^+ clays are added, the two Tg still exist at near the positions. As expected, when the addition of Cloisite 20A clays are added the two Tg becomes the single Tg, about 128 °C. We also measure the Tg of the blend with RDP-coated clays. From the figure we can see that the addition of RDP-coated clays obtains a single Tg, which is about 122 °C. Thus, the formation of single Tg could result from an increase of the compatibility, which is a good agreement with both the TEM and STXM images. In addition, the measurements of dynamic modulus as a function of temperature could explain that the RDP-coated clays act as a compatibilizer. From the Figure 16b we can see that in the case of RDP-coated clays the storage modulus gradually decreases as temperature increases compared to the others clays, where the storage modulus are constant up to 95 °C. This difference on the modulus could result from the extra RDP oligomers in the clay galleries. It could lead to an increase of loss modulus during heating. Therefore, the addition of RDP-coated clays could make the polymer matrix ductile, which may increase impact toughness of the polymer blend.

3.3. Application. *Cone Calorimetry*. As has been discussed in several previous publications,[6,7] rendering polymer blends flame retardant can pose a significant challenge. The combustion behaviors of polymers involve a complex sequence of condensed and gas phase reactions. In blends, the additional phase segregation during heating further complicates the situation and degrades the resistance to combustion. We have previously shown that the addition of Cloisite clays can stabilize blends against phase segregations and catalyze reactions that lead to chars formation. In the case where exfoliation occurred in at least one of the components, the addition of organoclays was observed to decrease the heat release rate (HRR) and mass loss rate (MLR).[6,7,45]

Here, we will compare the flame retardant properties of blends where the RDP clays have been added, rather than the Cloisite organoclays. In Figure 17a,b, we show the HRR and MLR of the PC/SAN24 blends performed in nitrogen atmosphere. From the figure, we find that the addition of Cloisite 20A only decreases the maximum HRR slightly but has nearly no effect on the MLR. In fact, a closer examination of the time dependence shows that Cloisite 20A degrades the performance of flame retardancy and decreases the total heat loss and mass loss time, which is somewhat consistent with the previous reports that the ditallow coating of the organoclays

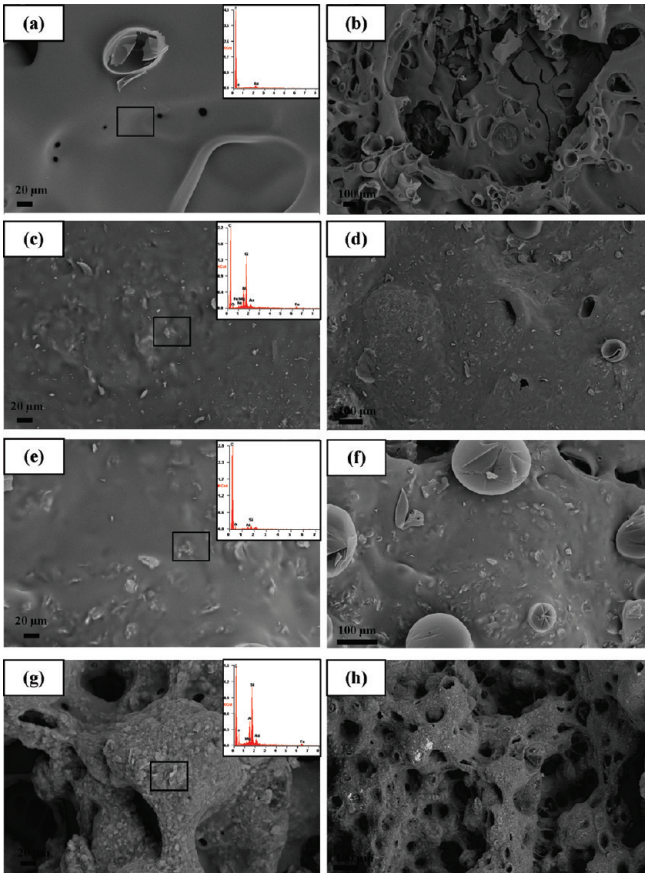

Figure 19. The SEM images and inserted EDAX spectra from the residues after the gasification test: (a,b) PC/SAN24 (50/50 wt %), (c,d) PC/SAN24/Cloisite Na^+ (50/50/5 wt %), (e,f) PC/SAN24/RDP MMT-Na^+ (50/50/5 wt %), and (g,h) PC/SAN24/Cloisite 20A (50/50/5 wt %).

is combustible and can decrease the time to ignition in nanocomposites.[6,7] The addition of MMT-Na^+ clays improves the performance, but the addition of RDP-coated MMT-Na^+ clays indicates a major improvement on the HRR and the MLR. From the figure, we find that the peak HRR is decreased by more than a factor of 2, and the MLR is decreased by 30%, while the total combustion time is nearly the same amount in the PC/SAN24 blend. This behavior also appears to be correlated to the characteristics of the chars, which can be seen in video clips obtained during the gasification test (see Supporting Information). PC is known to be a good char former even though styrenic copolymers such as SAN are not. All blends, with and without clays, are observed to form chars, and the amount of carbonaceous chars were calculated after subtracting the inorganic components, which are listed in Table 4 and Table 5. From the tables, we can see that the largest amount of char residues is found in the unfilled blend, while the addition of clays reduces the total carbonaceous chars by more than 45%, regardless of the type of clays. Hence the difference in the flame retardant performance with the addition of clays is not strictly a function of the ability to form char.

In Figure 18, we show still images of the samples obtained from the video clips. From the figure, we find that the char forms very quickly and then begins to swell with the gases from thermal decomposition of the blend and finally builds up the pressure inside. In the case of the unfilled blend and that containing RDP clays, a decrease in both MLR and HRR is observed when the char becomes thick enough to contain the gases and a "mushroom" structure is formed.

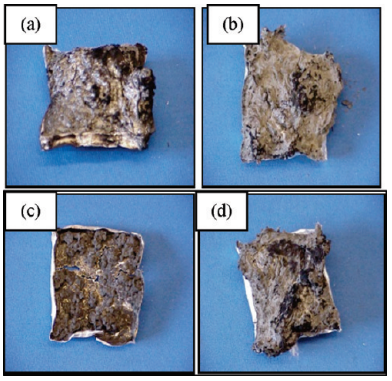

Figure 20. The images of residues left after the gasification test: (a) PC/SAN24 (50/50 wt %), (b) PC/SAN24/Cloisite Na+ (50/50/5 wt %), (c) PC/SAN24/Cloisite 20A (50/50/5 wt %), and (d) PC/SAN24/RDP MMT-Na^+ (50/50/5 wt %).

In the case of the blend containing Cloisite 20A, the char collapses very quickly when the gases build up and no mushroom-like structures is formed. As a result, the thermal decomposition progresses very quickly and no reduction in the MLR and the HRR is observed.

The morphology of the chars was further studied using SEM and EDAX. In Figure 19, we show the chars formed in the blend without clay. The box signifies the location where EDAX analysis was performed. In the EDAX spectrum, we find primarily carbon, which is expected in the char. The morphology image at 20 μm magnifications shows that the char is fairly uniform, while the image at 100 μm magnification shows with what appear to be "vent holes" type of formations. Some of these "vents" are covered with membranes, while others have ruptured membranes or membranes blown away. This morphology is consistent with the "mushroom" observed to form in the optical images. As the mushroom forms, the rate of gases released decreases but is not completely stopped. The SEM images show that a uniform char layer is formed, but the gases can still escape from the holes. The chars from the blends with RDP or MMT clays have similar morphologies with what appear to be membrane-covered vent holes. The high-magnification images show a uniform structure, which the EDAX spectra indicate that the membrane is mostly carbonaceous material. The Si/Mg/Al peaks, which are characteristic of the clays, are very small in comparison to the C peak from the char. Since the clay platelets do not decompose and are still in the char, the EDAX spectra indicate that they must either be in the interior of the chars or remain dispersed within the surface layer (at the 5% level) allowing the carbonaceous "skin" to form. Not surprisingly the appearance of this "skin" is similar to that observed in the blend without clays.

The images of the char with the Cloisite 20A clays are shown in Figure 19 where a sharp contrast is immediately observed. The high-magnification image shows that the structure of the char is almost entirely composed of compacted clay platelets. This is confirmed by the EDAX image, where the Al/Mg/Si peaks predominate and only a small C peak is observed. These images indicate that upon heating, the Cloisite 20A clays segregate to the surfaces of the sample, possibly due to the large unfavorable energy with the matrix. In contrast to the previously reported results for PS/PMMA, where the polymer did not form a char and the clay "char" was the only means of preventing heat and mass loss, in this case the PC/SAN blend does form a good char. The clays appear to interfere with this char layer. The large-magnification image shows that the morphology of this resultant char

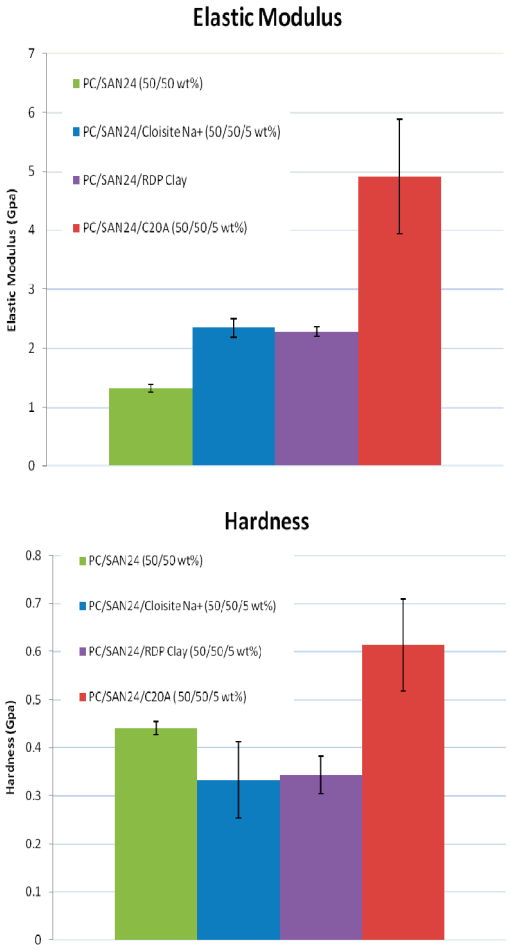

Figure 21. The hardness and elastic modulus of the residues from the gasification test.

is very porous, as opposed to the char of the pure blends. The high degree of porosity is consistent with the inability of this char layer to contain the combustion gases, resulting in the poor flame retardant behavior.

Another factor that may impede the formation of the "mushroom" structure is the hardness and the elastic modulus of the chars. For the mushroom structure to expand, while containing the gases, the material must be relatively elastic; otherwise the internal pressure will produce cracks, which release the gases and accelerate combustion. We therefore used nanoindentiation to measure both the elastic modulus and the hardness of the chars (shown in Figure 20). The results of the nanoidentation tests are shown in Figure 21. From the figure, we can see that the modulus of the char formed by the unfilled blend is the smallest, $E' = 1.3$ GPa, while its hardness is intermediate. The unfilled blend is able to form an intumescing char, but the larger hardness to modulus ratio indicates that it is somewhat brittle and, as can be seen in the images, unstable. Hence the flame retardant performance is not satisfactory. The addition of Cloisite 20A deteriorates the performance even further. Here we can see that the modulus, as well as the hardness, is nearly 400% larger than for the other materials, and the mushroom-like structures are unable to form altogether. The modulus that we measure, $E' = 4.9$ GPa, is larger than $E' = 2.3$ GPa of the Cloisite Na^+ or the RDP clays-filled system but still smaller than that of pure montmorillonite clays $E' = 14$ GPa,[46,47] indicating that despite the high concentration of clays, there may be other deposits of the polymer char left. The chars formed by the Cloisite Na^+ and RDP clays have similar hardness and modulii, where the modulii are larger than that of the pure blend, but the hardness is lower, indicating more elastic behavior. In both cases, the mushroom-like structures are able to form which contain the gases. We can only postulate, therefore, the superior flame retardant responses of the blends containing the RDP clays over those containing the Na^+ clays may be the presence of the adsorbed RDP on the clay surfaces, which catalyzes the reactions needed for further reduction of the HRR and MLR.

4. Conclusion

The absorption of RDP oligmoers on clay surfaces has been proposed as a replacement for ditallow molecules commonly used in functionalizing clays. Using SAXS, we showed that RDP can be adsorbed on the surfaces of sodium montmorillonite clays, thereby increasing the interlayer spacing from 1.25 to 2.23 nm. We then demonstrated, using SAXS and TEM, that these modified clays can be exfoliated in styrenic polymers, HIPS and ABS, as well as in PP. We also produced single layers of the clays, using the LB technique and measured the contact angle of polymers on the surface, which were consistent with the ability to exfoliate. We found that the contact angle between PS/RDP clays substrate was ~2.5°, whereas the angle for PS/Cloisite 20A clays substrate was ~32°. Therefore, the RDP-coated clays were more compatible to the styrene groups compared to the Cloisite clays, which could lead to the exfoliation of HIPS and ABS.

The ability of RDP-coated clays to compatibilize polymer blends was also probed. We showed that RDP-coated clays segregated to the interfaces between the phase domains in the PC/SAN24 blend, while they segregated inside the PMMA domains in the PS/PMMA blend. This different morphology between the two blends could be explained by the interfacial energy. Since the interfacial tension for either PMMA/RDP or PS/RDP clays (~2.8 mN/m at 180 °C) was higher than that for PS/PMMA interfaces (~1.2 mN/m at 180 °C) the segregations of RDP-coated clays could not reduce the interfacial energy of the system. However, the interfacial energy for PC/SAN24 blend (~2.8 mN/m at 200 °C) was much higher than the interfacial tension for PC/RDP clays (~0.5 mN/m if $S = 0$). Hence segregation of the RDP clays to the interfaces resulted in a significant reduction of the overall energy and increased compatibilization.

We also compared the effects of RDP-coated clays on the flame retardant properties of the PC/SAN24 blend. We found that the addition of the RDP clays could reduce the HRR and MLR for the blends in which they were interfacial active. In contrast, the Cloisite clays, which were also interfacial active, were shown to deteriorate the flame retardant responses. In addition to stability against phase segregation, the quality of chars is another important criterion for flame retardance. We show that elasticity is an important consideration in intumescing chars, which have to expand to contain the gases formed by the advancing heat front. TEM images indicated that the Cloisite clays segregated to the surfaces of the chars, while the RDP-coated clays remained in the interior. Nanoindentation measurements showed that the clay rich surface crust resulted in the chars of the nanocomposites containing Cloisite 20A to be 400% more brittle than those resulting from the compounds with the RDP or Na^+ clays. These results show that surfaces, as well as interfacial energies, have to be considered in engineering the optimal properties of nanocomposites, and furthermore that clays treated with nonhalogen (FR) oligomers can be an alternative for replacing the functionalized clays treated with the ditallow molecules.

Acknowledgment. The authors thank Ms. Susan C. Van Horn from Central Microscopy Imaging Center (C-MIC) at Stony

Brook University for taking TEM images. This work was supported by the NSF-MRSEC program, the AERTC through a grant from Brookhaven National Laboratory and a grant from ICL-Supresta. The authors also thank NSF award CMMI-0626025 for partial support of this work.

Supporting Information Available: This material is available free of charge via the internet at http://pubs.acs.org.

References and Notes

(1) Balazs, A. C.; Emrick, T.; Russell, T. P. *Science* **2006**, *314*, 1107–1110.
(2) Gelfer, M.; Burger, C.; Fadeev, A.; Sics, I.; Chu, B.; Hsiao, B. S.; Heintz, A.; Kojo, K.; Hsu, S.-L.; Si, M.; Rafailovich, M. *Langmuir* **2004**, *20*, 3736–3758.
(3) Vaia, R. A.; Giannelis, E. P. *Macromolecules* **1997**, *30*, 7990–7999.
(4) Vaia, R. A.; Giannelis, E. P. *Macromolecules* **1997**, *30*, 8000–8009.
(5) Starr, F. W.; Schroder, T. S.; Glotzer, S. C. *Macromolecules* **2002**, *35*, 4481–4492.
(6) Pack, S.; Si, M.; Koo, J.; Sokolov, J. C.; Koga, T.; Kashiwagi, T.; Rafailovich, M. H. *Polym. Degrad. Stab.* **2009**, *93*, 306–326.
(7) Pack, S.; Kashiwagi, T.; Stemp, D.; Koo, J.; Si, M.; Sokolov, J. C.; Rafailovich, M. H. *Macromolecules* **2009**, *42*, 6698–6707.
(8) Wang, Y.; Zhang, Q.; Fu, Q. *Macromol. Rapid Commun.* **2003**, *24*, 231–235.
(9) Khatu, B. B.; Lee, D.; Kim, H.; Kim, J. *Macromolecules* **2004**, *37*, 2454–2459.
(10) Li, Y.; Shimizu, H. *Macromol. Rapid Commun.* **2005**, *26*, 710–715.
(11) Yoo, Y.; Park, C.; Lee, S.; Choi, K.; Kim, D.; Lee, J. *Macromol. Chem. Phys.* **2005**, *206*, 878–884.
(12) Ray, S. S.; Pouliot, S.; Bousmina, M.; Utracki, L. A. *Polymer* **2004**, *45*, 8403–8413.
(13) Nesterov, A. E.; Lipatov, Y. S. *Polymer* **1999**, *40*, 471–481.
(14) Lipatov, Y. S.; Nesterov, A. E.; Ignatova, T. D.; Nesterov, D. A. *Polymer* **2002**, *43*, 875–880.
(15) Si, M.; Araki, T.; Ade, H.; Kilcoyne, A. L. D.; Fisher, R.; Sokolov, J. C.; Rafailovich, M. H. *Macromolecules* **2006**, *39*, 4793–4801.
(16) Koo, J.; Park, S.; Satija, S.; Tikhonov, A.; Sokolov, J. C.; Rafailovich, M. H.; Koga, T. J. *Colloid Interface Sci.* **2008**, *318*, 103–109.
(17) Vaia, R. A.; Teukolsky, R. K.; Giannelis, E. P. *Chem. Mater.* **1994**, *6*, 1017–1022.
(18) Xie, W.; Gao, Z.; Pan, W.; Hunter, D.; Singh, A.; Vaia, R. *Chem. Mater.* **2001**, *13*, 2979–2990.
(19) Zhu, J.; Uhl, F. M.; Morgan, A. B.; Wilkie, C. A. *Chem. Mater.* **2001**, *13*, 4649–4654.
(20) Zeng, C.; Lee, L. J. *Macromolecules* **2001**, *34*, 4098–4103.
(21) Chen, B.; Evans, R. G. *Carbohydr. Polym.* **2005**, *61*, 455–463.
(22) Hou, S.; Schmidt-Rohr, K. *Chem. Mater.* **2003**, *15*, 1938–1940.
(23) Sarkar, M.; Dana, K.; Ghatak, S.; Banerjee, A. *Bull. Mater. Sci.* **2008**, *31*, 23–28.
(24) Ramazani, A.; Tavakolzadeh, F.; Baniasadi, H. *J. Appl. Polym. Sci.* **2009**, *115*, 308–314.
(25) Modro, A. M.; Modro, T. A. *Can. J. Chem.* **1999**, *77*, 890–894.
(26) Jang, B.; Wilkie, C. A. *Thermochim. Acta* **2005**, *433*, 1–12.
(27) Granzow, A. *Acc. Chem. Res.* **1978**, *11*, 177–183.
(28) Ade, H.; Smith, A. P.; Cameron, S.; Cieslinski, R.; Mitchell, G.; Hsiao, B.; Rightor, E. *Polymer* **1995**, *36*, 1843–1848.
(29) Ade, H.; Winesett, D. A.; Smith, A. P.; Qu, S.; Ge, S.; Sokolov, J.; Rafailovich, M. *Europhys. Lett.* **1999**, *45*, 526–532.
(30) Qu, S.; Clarke, C. J.; Liu, Y.; Rafailovich, H. M.; Sokolov, J.; Phelan, K. C.; Krausch, G. *Macromolecules* **1997**, *30*, 3640–3645.
(31) Oliver, W. C.; Pharr, G. M. *J. Mater. Res.* **1992**, *7*, 1564–1583.
(32) Krishnamoorti, R.; Vaia, R. A.; Giannelis, E. *Chem. Mater.* **1996**, *8*, 1728–1734.
(33) Vaia, R. A.; Ishii, H.; Giannelis, E. P. *Chem. Mater.* **1993**, *5*, 1694–1696.
(34) Murashko, E. A.; Levchik, G. F.; Levchik, S. V.; Bright, D. A.; Dashevsky, S. *J. Fire. Sci.* **1998**, *16*, 278–295.
(35) Cole, K. C. *Macromolecules* **2008**, *41*, 834–843.
(36) Yan, L.; Roth, C. B.; Low, P. F. *Langmuir* **1996**, *12*, 4421–4429.
(37) Wu., S. *J. Phys. Chem.* **1970**, *74*, 632–638.
(38) Wyart, F. B.; Martin, P.; Redon, C. *Langmuir* **1993**, *9*, 3682–3690.
(39) Carriere, C. J.; Biresaw, G.; Sammler, R. L. *Rheol. Acta* **2000**, *39*, 476–482.
(40) Zhang, X.; Kim, J. *Macromol. Rapid Commun.* **1998**, *19*, 499–504.
(41) Valera, T. S.; Morita, A. T.; Demarquette, N. R. *Macromolecules* **2006**, *39*, 2663–2675.
(42) Faldi, A.; Composto, R. J.; Winey, K. I. *Langmuir* **1995**, *11*, 4855–4861.
(43) Watkins, V. H.; Hobbs, S. Y. *Polymer* **1993**, *34*, 3955–3959.
(44) Hobbs, S. Y.; Dekkers, E. J.; Watkins, V. H. *Polymer* **1998**, *29*, 1598–1602.
(45) Kashiwagi, T.; Mu, M; Winey, K. I.; Cipriano, B.; Raghavan, S.; Pack, S.; Rafailovich, M.; Yang, Y.; Grulke, E.; Shields, J.; Harris, R.; Douglas, J. *Polymer* **2008**, *49*, 4358–4368.
(46) Vanorio, T.; Prasad, M.; Nur, A. *Geophys. J. Int.* **2003**, *155*, 319–326.
(47) Chen, B.; Evans, J. R. G. *Scr. Mater.* **2006**, *54*, 1581–1585.